OPTICS

Topological nature of nonlinear optical effects in solids

10.1126/sciadv.1501524

Takahiro Morimoto[1]* and Naoto Nagaosa[2,3]

There are a variety of nonlinear optical effects including higher harmonic generations, photovoltaic effects, and nonlinear Kerr rotations. They are realized by strong light irradiation to materials that results in nonlinear polarizations in the electric field. These are of great importance in studying the physics of excited states of the system as well as for applications to optical devices and solar cells. Nonlinear properties of materials are usually described by nonlinear susceptibilities, which have complex expressions including many matrix elements and energy denominators. On the other hand, a nonequilibrium steady state under an electric field periodic in time has a concise description in terms of the Floquet bands of electrons dressed by photons. We show theoretically, using the Floquet formalism, that various nonlinear optical effects, such as the shift current in noncentrosymmetric materials, photovoltaic Hall response, and photo-induced change of order parameters under the continuous irradiation of monochromatic light, can be described in a unified fashion by topological quantities involving the Berry connection and Berry curvature. We found that vector fields defined with the Berry connections in the space of momentum and/or parameters govern the nonlinear responses. This topological view offers a route to designing nonlinear optical materials.

INTRODUCTION

Under strong light irradiation, materials show electric polarization $\mathcal{P}$ or current $J = d\mathcal{P}/dt$, which are nonlinear functions of the electric field E. These nonlinear optical responses (NLORs) form one of the most important research fields in condensed matter physics (*1*, *2*) because nonlinearity often plays a crucial role in optical devices. NLORs are also of crucial importance for solar cell action. The photocurrent in a solar cell is usually described by two processes: the generation of electron-hole pairs or excitons and the separation of electrons and holes by the potential gradient in the p-n junctions. A remarkable recent advance is the discovery of the large efficiency of solar cell action in perovskite oxides with noncentrosymmetric crystal structure (*3*–*7*). One promising scheme that describes this phenomenon is the shift current induced by the band structure without inversion symmetry (*8*–*11*).

Although the nonlinear optical processes described above involve high-energy excited states, the ground state and low-energy excited states are sometimes characterized by the topological nature of the Bloch wave functions. Specifically, the Berry connection and curvature of wave functions determine the ground-state properties and low-energy transport phenomena. Such examples include ferroelectricity (*12*), quantum Hall effect (*13*, *14*), anomalous Hall effect (*15*), spin Hall effect (*16*, *17*), topological insulators (*18*–*20*), and ideal dc conduction (*21*). Quantum mechanical wave functions can be regarded as geometrical objects in the Hilbert space because the inner product and distance are defined for them. This is the case especially in solids because the Bloch wave functions are grouped into several bands separated by energy gaps, and each band n is regarded as a manifold in the Hilbert space. This manifold is characterized by a connection $\boldsymbol{a}_n(\boldsymbol{k})$ that relates two neighboring wave functions in the crystal momentum (k-)space as

$$\boldsymbol{a}_n(\boldsymbol{k}) = -i\langle u_{n\boldsymbol{k}}|\nabla_{\boldsymbol{k}} u_{n\boldsymbol{k}}\rangle \tag{1}$$

where $|u_{n\boldsymbol{k}}\rangle$ is the periodic part of the Bloch wave function. One can also extend this concept to a generalized space including some parameters Q characterizing the Hamiltonian, such as atomic displacement. Equation 1 has the meaning of the intracell coordinates (*22*), where the real-space coordinate $\boldsymbol{x}_c$ of the wave packet made from the Bloch wave functions near $\boldsymbol{k}$ is represented by

$$x_c^{\mu} = i\frac{\partial}{\partial k_{\mu}} - a_n^{\mu}(\boldsymbol{k}) \tag{2}$$

The second term comes from the nontrivial connection of the manifold for the band n and upgrades the usual derivative in $\boldsymbol{k}$ to the gauge covariant derivative, which is physically observable. Although $a_n^{\mu}(\boldsymbol{k})$ is a gauge-dependent quantity (subject to a change of phases of wave functions), this correction can be understood as a band-dependent shift of the electron position arising from different linear combinations of atomic orbitals in the unit cell (*22*). We note here that the vector potential $a_n^{\mu}(\boldsymbol{k})$ is related to the real-space position because of the canonical conjugation relationship between $\boldsymbol{x}$ and $\boldsymbol{k}$.

The quantum Hall effect is a famous example where the geometry of wave functions plays a crucial role in low-energy transport. The Hall conductivity σ_{xy} can be represented by the integral of the Berry curvature $\mathcal{F}_n(\boldsymbol{k}) \equiv [\nabla_{\boldsymbol{k}} \times \boldsymbol{a}_n(\boldsymbol{k})]_z$ over the occupied states (*13*). In the case of an insulator, the integral with respect to $\boldsymbol{k}$ over the first Brillouin zone is quantized and called the Chern number. This leads to the quantized σ_{xy}, that is, the (integer) quantum Hall effect. By replacing one of the momenta, for example, k_y, by some parameter Q characterizing the Hamiltonian, σ_{xy} turns into the electric polarization induced by the change in Q (*12*). A nonvanishing Chern number in the $\boldsymbol{k}Q$-space is tied to the quantum pumping (*14*).

However, these topological characterizations have been limited to ground-state properties or linear responses to the weak external stimuli of low frequency. This is because NLORs involve higher-energy excitations such as particle-hole pairs, which drive the quantum state out of the ground-state manifold. Conventional descriptions of the nonlinear

[1]Department of Physics, University of California, Berkeley, Berkeley, CA 94720, USA. [2]RIKEN Center for Emergent Matter Science (CEMS), Wako, Saitama 351-0198, Japan. [3]Department of Applied Physics, University of Tokyo, Tokyo 113-8656, Japan. *Corresponding author. Email: tmorimoto@berkeley.edu

responses are given by nonlinear susceptibility tensors χ's whose independent components are specified by the crystal symmetry and the time-reversal symmetry (TRS). Microscopically, tensors χ's have complex expressions including many matrix elements of the dipole moment along with energy denominators. These expressions usually do not give much information except for the trivial fact that the nonlinear responses show a resonance effect when the energy of light is nearly equal to the energy difference between the two states connected by the matrix elements. The topological nature of responses to the strong- and/or high-frequency stimuli has not been explored thus far except for a few cases.

The shift current is one of these few nonlinear phenomena whose geometrical meaning has been studied. The photocurrent is the current induced by light irradiation, as is well known. The induced photocurrent J is usually proportional to E^3 when the system preserves the inversion symmetry. However, when the system lacks inversion symmetry, the photocurrent J can be proportional to E^2, and it is called "shift current." von Baltz and Kraut (*8*) have derived a formula for this shift current and related it to the intracell coordinates mentioned above. Specifically, it is expressed in terms of the phase $\varphi_{ij}(\boldsymbol{k})$ of the velocity matrix element $v_{ij}(\boldsymbol{k})$ between the valence and conduction bands and the Berry connection $\boldsymbol{a}_n(\boldsymbol{k})$ as

$$\boldsymbol{J} \propto E^2 \int d\boldsymbol{k} \delta\left(\epsilon_1(\boldsymbol{k}) - \epsilon_2(\boldsymbol{k}) + \hbar\omega\right) \times \left|v_{12}(\boldsymbol{k})\right|^2 \left[\nabla_{\boldsymbol{k}} \varphi_{12}(\boldsymbol{k}) + \boldsymbol{a}_1(\boldsymbol{k}) - \boldsymbol{a}_2(\boldsymbol{k})\right] \quad (3)$$

where subscripts 1 and 2 refer to the valence band and the conduction band, respectively, $\epsilon_i(\boldsymbol{k})$ is the energy of the band, and $\hbar\omega$ is the energy of the incident light. Note that this expression is gauge-invariant due to the combination of $\nabla_{\boldsymbol{k}}\varphi_{12}(\boldsymbol{k})$ and $\boldsymbol{a}_{1,2}(\boldsymbol{k})$, and it is remarkable in a sense that the vector potential itself appears in the physical quantities. It is considered as a candidate mechanism of the high-efficiency photovoltaic current in the solar cell action without the *p-n* junction (*3–7*, *9–11*). We note that the photovoltaic Hall effect of two-dimensional (2D) Dirac fermions (for example, in graphene) has also been studied as a topological phenomenon (*23–27*), where the circularly polarized light induces Hall conductance σ_{xy} proportional to E^2. In this case, the current J is the third-order effect, that is, $\propto E^3$. We show that the light-induced σ_{xy} is expressed by a similar formula to that for the linear response; the only modification in the expression for σ_{xy} is that $\mathcal{F}_n(\boldsymbol{k})$ and the Fermi distribution function are replaced by those of the nonequilibrium Floquet bands.

Here, we study the topological nature of the NLORs by using the Floquet two-band models. This formalism offers a general description of nonlinear responses when the following conditions are met: (i) only one frequency Ω is involved (monochromatic light), (ii) mostly two bands are involved in the optical transitions, and (iii) a steady state is achieved. We show that NLORs of the even order of the external electric field E, such as photovoltaic effects and second-harmonic generations (SHGs), have geometrical meaning and are characterized by the Berry connection in a generalized space including both the momentum $\boldsymbol{k}$ and parameter Q. In particular, we point out that this topological description is applicable to general noncentrosymmetric crystals that support the even-order nonlinear responses. We also discuss the fact that nonlinear dc Hall responses, which are nonlinear responses in the odd order of E in general, are related to the Berry curvature of Floquet bands. (Note, however, that the topological description is limited to the dc output in this case of odd-order responses.) Moreover, we classify the nonlinear processes according to the presence or absence of inversion symmetry (P) and TRS (T) in terms of the Berry connection and the Berry curvature.

To demonstrate our general discussions, we apply our formalism to a 1D model with inversion symmetry breaking, which is a simple model of ferroelectric materials. By doing so, we clarify the topological nature of a few nonlinear responses and the symmetry constraints to the nonlinear responses in an explicit way.

RESULTS

Floquet two-band model

We study nonlinear current responses by using the Keldysh Green's function method combined with the Floquet formalism (*28–31*). (See Materials and Methods for details of the formalism.) We focus on the two bands involved in the transition induced by monochromatic light with an electric field $E(t) = Ee^{-i\Omega t} + E^* e^{i\Omega t}$. By using the Floquet bands, one can describe the nonequilibrium steady state as an anticrossing of a valence band dressed with one photon and a conduction band dressed with no photon, which is schematically shown in Fig. 1. The anticrossing of these two Floquet bands is captured by the following Hamiltonian (the convention $\hbar = 1$, $e = 1$ is used hereafter)

$$H_F = \begin{pmatrix} \epsilon_1^0 + \Omega & -iA^* v_{12}^0 \\ iAv_{21}^0 & \epsilon_2^0 \end{pmatrix} \equiv \epsilon + \boldsymbol{d} \cdot \boldsymbol{\sigma} \quad (4)$$

where subscripts 1 and 2 refer to the valence band and the conduction band, respectively, ϵ^0 is the original energy dispersion (for $E = 0$), $A = E/\Omega$, and $v^0 = \partial H_0(A = 0)/\partial k$. The dc current operator is given by

$$\tilde{v} = \frac{\partial H_F}{\partial k} \begin{pmatrix} v_{11}^0 & -iA^* \left(\frac{\partial v^0}{\partial k}\right)_{12} \\ iA\left(\frac{\partial v^0}{\partial k}\right)_{21} & v_{22}^0 \end{pmatrix} \equiv b_0 + \boldsymbol{b} \cdot \boldsymbol{\sigma} \quad (5)$$

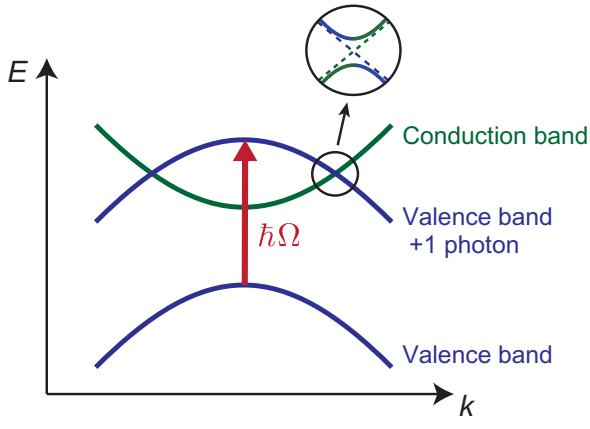

Fig. 1. Schematic picture of the Floquet two band model. Under the drive of monochromatic light, energy bands evolve into Floquet bands, which describe Bloch states dressed with photons. When two Floquet bands cross, they show an anticrossing. The nonequilibrium steady state (and hence, NLORs) can be captured by studying this anticrossing of two Floquet bands.

Physical quantities are obtained from the lesser Green's function, which is given for the two-band model as

$$G^{<} = \frac{(\omega - \epsilon + i\Gamma/2 + \boldsymbol{d}\cdot\boldsymbol{\sigma})\Sigma^{<}(\omega - \epsilon - i\Gamma/2 + \boldsymbol{d}\cdot\boldsymbol{\sigma})}{[(\omega - \epsilon + i\Gamma/2)^2 - d^2][(\omega - \epsilon - i\Gamma/2)^2 - d^2]} \quad (6)$$

Here, the lesser self-energy is given by $\Sigma^{<} = i\Gamma(1 + \sigma_z)/2$. This form of $\Sigma^{<}$ assumes that the system couples to a heat bath, which has a uniform energy spectrum and Fermi energy lying within the energy gap of the system.

Thus, we obtain the dc current expectation value as

$$J = -i\mathbf{Tr}(\tilde{v}G^{<}) = \int d\boldsymbol{k}(j_1 + j_2 + j_3) \quad (7)$$

with

$$j_1 = \frac{\frac{\Gamma}{2}(-d_x b_y + d_y b_x)}{d^2 + \frac{\Gamma^2}{4}} \quad (8)$$

$$j_2 = \frac{(d_x b_x + d_y b_y)d_z}{d^2 + \frac{\Gamma^2}{4}} \quad (9)$$

$$j_3 = \frac{\left(d_z^2 + \frac{\Gamma^2}{4}\right)b_z}{d^2 + \frac{\Gamma^2}{4}} + b_0 \quad (10)$$

where Tr denotes an integration over ω and k and a trace for two by two matrices.

The first term j_1 in Eq. 7 can be written with the Berry phase as follows. First, we write the denominator as

$$\begin{aligned} -d_x b_y + d_y b_x &= \mathrm{Im}[(d_x + id_y)(b_x - ib_y)] \\ &= |A|^2 \mathrm{Im}\left[v_{21}^0 \left(\frac{\partial v^0}{\partial k}\right)_{12}\right] \end{aligned} \quad (11)$$

with the current operator v^0 for the system without driving by E. In the two-band model, the matrix element of $\frac{\partial v^0}{\partial k}$ is written as

$$\begin{aligned} \left(\frac{\partial v^0}{\partial k}\right)_{12} &= \frac{\partial v_{12}^0}{\partial k} - \langle \partial_k u_1 | v^0 | u_2 \rangle - \langle u_1 | v^0 | \partial_k u_2 \rangle \\ &= v_{12}^0 \left[\frac{\partial}{\partial k} \log v_{12}^0 + i a_1 - i a_2 + \frac{v_{11}^0 - v_{22}^0}{\epsilon_1 - \epsilon_2}\right] \end{aligned} \quad (12)$$

with $a_i = -i\langle u_i | \partial_k u_i \rangle$. Here, we used the identity $|u_1\rangle\langle u_1| + |u_2\rangle\langle u_2| = 1$ for the two-band model, and $\langle u_1 | \partial_k u_2 \rangle = -v_{12}^0/(\epsilon_1 - \epsilon_2)$. Thus, we obtain

$$d_x b_y - d_y b_x = |A|^2 |v_{12}^0|^2 R_k \quad (13)$$

$$R_k = \left[\frac{\partial \varphi_{12}}{\partial k} + a_1 - a_2\right] \quad (14)$$

with $\varphi_{12} = \mathrm{Im}(\log v_{12}^0)$ because a_i and v_{ii}^0 are real. The vector R_k is called a shift vector, which measures the difference of intracell coordinates between the two bands involved in the resonance. We note that R_k is a gauge-invariant quantity, where the Berry connection accompanies the k-derivative of the velocity operator to compensate the nontrivial parallel translation for the Bloch wave functions in k. Then, the contribution to the current expectation value is written as

$$\begin{aligned} j_1 &= |A|^2 \frac{\frac{\Gamma}{2}}{d_z^2 + |A|^2 |v_{12}^0|^2 + \frac{\Gamma^2}{4}} |v_{12}^0|^2 R_k \\ &\cong \frac{\pi |E|^2}{\Omega^2} \frac{\frac{\Gamma}{2}}{\sqrt{\frac{|E|^2 |v_{12}^0|^2}{\Omega^2} + \frac{\Gamma^2}{4}}} \delta(d_z) |v_{12}^0|^2 R_k \end{aligned} \quad (15)$$

where we have assumed in the second line that Γ and $|Av_{12}^0|$ are much smaller than the energy dispersion. If we further assume sufficiently small electric fields ($|Av_{12}^0| \ll \Gamma$), this reduces to $j_1 \cong \frac{\pi |E|^2}{\Omega^2} \delta(d_z) |v_{12}^0|^2 R_k$. The second term j_2 in Eq. 7 is rewritten by using $d_x b_x + d_y b_y = |A|^2 \mathrm{Re}\left[v_{21}^0 \left(\frac{\partial v^0}{\partial k}\right)_{12}\right]$ as

$$j_2 = \frac{|A|^2 \mathrm{Re}\left[v_{21}^0 \left(\frac{\partial v^0}{\partial k}\right)_{12}\right] d_z}{d^2 + \frac{\Gamma^2}{4}} \quad (16)$$

This contribution vanishes after integration over k in the presence of the TRS, because j_2 is odd under the TRS. This can be understood from Eq. 12 and the fact that v_{ii}^0 is odd under the TRS. In a similar way, the contribution of j_3 in Eq. 7 vanishes because j_3 is odd under the TRS.

To summarize, the photocurrent in the second order of E is given by

$$J = \frac{\pi |E|^2}{\Omega^2} \int d\boldsymbol{k} \delta(\epsilon_1^0 - \epsilon_2^0 + \hbar\omega) |v_{12}^0|^2 [\partial_k \varphi_{12} + a_1 - a_2] \quad (17)$$

in the presence of the TRS, which reproduces the expression for the shift current (*8*, *9*, *32*). Although we have focused on the two-band model, the result in Eq. 17 can be extended to general cases involving more energy bands by summing up contributions from any two bands satisfying the resonance condition. We note that higher-order correction to the above formula is captured by the factor $\frac{\Gamma}{2} / \sqrt{\frac{|E|^2 |v_{12}^0|^2}{\Omega^2} + \frac{\Gamma^2}{4}}$ in Eq. 15.

This leads to a crossover of photocurrent from $J \propto E^2$ to $J \propto \Gamma E$ by increasing the intensity of the monochromatic light and describes the effect of saturation of excitations.

Second-harmonic generation

The SHG is the nonlinear current response with the frequency 2Ω induced by a monochromatic light $E(t) = Ee^{-i\Omega t} + E^* e^{i\Omega t}$. We show that the SHG is also described with geometrical quantity (that is, Berry connections) in a similar manner to the shift current. Here, we consider the interband contribution to the SHG that involves

two energy bands in the optical transition. In this case, we can apply our approach based on the Floquet two-band model. Specifically, the SHG is contributed by two types of optical processes and accordingly two Floquet two-band models H_F in Eq. 4 and

$$H'_F = \begin{pmatrix} \epsilon_1^0 + 2\Omega & -\frac{1}{2}(A^*)^2\partial_k v_{12}^0 \\ -\frac{1}{2}A^2\partial_k v_{21}^0 & \epsilon_2^0 \end{pmatrix} \equiv d'_0 + \boldsymbol{d}' \cdot \boldsymbol{\sigma} \qquad (18)$$

The Floquet formalism also offers a concise description of time-dependent current responses, which is given in Eq. 36 in the Materials and Methods. According to Eq. 36, a contribution to $J(2\Omega)$, which is the Fourier component of the current proportional to $e^{-2i\Omega t}$, is written as $-iv'_{12}\,(G^<)_{21}$ for each Floquet two-band model, where v' is chosen to give the time dependence of $e^{-2i\Omega t}$. This is achieved by $v'_{12} = iA(\partial_k v^0)_{12}$ in the case of H_F and $v'_{12} = v^0_{12}$ in the case of H'_F. By using Eq. 48 for $(G^<)_{21}$, the interband contribution to the SHG is written as

$$J(2\Omega) \cong i\frac{E^2}{2\Omega^2}\int d\boldsymbol{k}|v_{12}^0|^2(\partial_k\varphi_{12} + a_1 - a_2)\left(-\frac{1}{d_z + \frac{i\Gamma}{2}} + \frac{1}{2\left(d'_z + \frac{i\Gamma}{2}\right)}\right) \qquad (19)$$

where we only kept nonvanishing terms in the presence of the TRS. In particular, if we focus on the contribution to the SHG by the interband resonance that involves a δ function with respect to the energy difference, this contribution is given by

$$J(2\Omega) \cong \frac{\pi E^2}{2\Omega^2}\int d\boldsymbol{k}|v_{12}^0|^2 R_k\left[-\delta(\epsilon_1^0 - \epsilon_2^0 + \Omega) + \frac{1}{2}\delta(\epsilon_1^0 - \epsilon_2^0 + 2\Omega)\right] \qquad (20)$$

This indicates that the interband contribution to the SHG is characterized by the shift vector R_k, which is defined with Berry connections. Thus, the SHG is generated by dynamics of an excited electron-hole pair that experiences a shift of intracell coordinates in the transition between the valence and the conduction bands and is naturally related to the Berry connection of the Bloch electron.

Third-order nonlinear response

Now, we proceed to the third-order nonlinear responses that are described by

$$J_i = \chi^3_{ij}E(\omega)E(-\omega)E_j(\omega = 0) \qquad (21)$$

Here, the current J_i is induced by the static electric field E_j in the presence of the pump laser light of the frequency ω.

We focus on the nonlinear Hall response in the 2D systems. The nonlinear Hall response is obtained by applying the linear response theory to the nonequilibrium steady states

$$\sigma_{xy} = \int_{BZ} d^2\boldsymbol{k}\sum_i f_i(\nabla \times \tilde{a}_i)_z \qquad (22)$$

and expanding it in the second power of $|E(\omega)|$ (*23*). Here, the Berry connection $\tilde{a}$ is defined for the Floquet states that describe the nonequilibrium steady states, and f_i is the occupation of the ith Floquet state. The wave functions of the Floquet two-band model in Eq. 4 are given by

$$u_1 = \begin{pmatrix} \cos\frac{\theta}{2} \\ \sin\frac{\theta}{2}e^{i\phi} \end{pmatrix}, \quad u_2 = \begin{pmatrix} -\sin\frac{\theta}{2} \\ \cos\frac{\theta}{2}e^{i\phi} \end{pmatrix} \qquad (23)$$

with

$$\cos\theta = \frac{d_z}{d}, \phi = \tan^{-1}\left(\frac{d_y}{d_x}\right) = \varphi_{21} \qquad (24)$$

Then, the Berry connections for Floquet bands u_1 and u_2 are given by

$$\tilde{\boldsymbol{a}}_1 = \frac{1}{2}(1 - \cos\theta)\nabla\phi + \cos^2\frac{\theta}{2}\boldsymbol{a}_1 + \sin^2\frac{\theta}{2}\boldsymbol{a}_2 \qquad (25)$$

$$\tilde{\boldsymbol{a}}_2 = \frac{1}{2}(1 + \cos\theta)\nabla\phi + \sin^2\frac{\theta}{2}\boldsymbol{a}_1 + \cos^2\frac{\theta}{2}\boldsymbol{a}_2 \qquad (26)$$

where a_1 and a_2 are Berry connections for the original bands with $E = 0$. The occupations are $f_1 = (1 + \cos\theta)/2$ and $f_2 = (1 - \cos\theta)/2$, because $f_i = (-i\Sigma^<_{ii})/\Gamma$ with $-i\Sigma^</\Gamma = (\sigma_z + 1)/2$. The original Hall conductivity σ^0_{xy} for $E = 0$ is given by setting $\theta = 0$. Then, one can obtain the photo-induced part of the Hall conductivity $\sigma^p_{xy} \equiv \sigma_{xy} - \sigma^0_{xy}$ as

$$\begin{aligned}\sigma^p_{xy} &= \frac{1}{4}\int d^2\boldsymbol{k}\sin^2\theta[\nabla \times (\nabla\phi + \boldsymbol{a}_2 - \boldsymbol{a}_1)]_z \\ &= \int d^2\boldsymbol{k}\frac{A^2|v_{12}^0|^2}{4(d_z^2 + A^2|v_{12}^0|^2)}\mathcal{F}\end{aligned} \qquad (27)$$

where $\mathcal{F} \equiv (\nabla \times \boldsymbol{a}_2 - \nabla \times \boldsymbol{a}_1)_z$. If we assume that A is sufficiently small, the Hall conductivity is given by

$$\sigma^p_{xy} = \int d^2\boldsymbol{k}\frac{\pi E}{4\Omega}|v_{12}^0|\delta(d_z)\mathcal{F} \qquad (28)$$

We can include the effect of relaxation by replacing the denominator in Eq. 27 with $4(d_z^2 + A^2|v_{12}^0|^2 + \Gamma^2)$, which leads to

$$\sigma^p_{xy} = \int d^2\boldsymbol{k}\frac{\pi E^2}{4\Gamma\Omega^2}|v_{12}^0|^2\delta(d_z)\mathcal{F} \qquad (29)$$

This photo-induced Hall conductivity is proportional to E^2 and describes the third-order nonlinear response. It is also proportional to the relaxation time $1/\Gamma$, indicating that the nonlinear modulation arises from excited free electrons. Equation 28 corresponds to the case of $A|v_{12}^0| \gg \Gamma$, whereas Eq. 29 corresponds to the case of $A|v_{12}^0| \ll \Gamma$. Therefore, these two equations describe the crossover from $\sigma^p_{xy} \propto E$ to $\propto E^2/\Gamma$ behaviors in a similar manner to the case of shift current.

This photo-induced Hall response is zero when the T-symmetry is preserved because in that case the contributions of $\mathcal{F}$ at $\boldsymbol{k}$ and $-\boldsymbol{k}$ cancel each other. It gives the correction to σ_{xy} in the T-broken case by the photoexcitation where $\mathcal{F}$ is the difference of the Berry curvatures between the conduction and the valence bands. This effect is extended to the nonlinear Kerr rotation when the probe electric field $E(\omega = 0)$ is replaced with that of nonzero frequency. In addition, it also expresses the effects that are finite even in the case of T-symmetric cases when one of $\boldsymbol{k}$-component is replaced by the parameter Q characterizing the Hamiltonian. Before discussing this issue, let us introduce an explicit model to demonstrate the NLORs.

Application to inversion symmetry broken 1D chains

We apply the formalism described above to a 1D model described by

$$H_0 = \sum_i \frac{1 + Q_2(-1)^i}{2}\left(e^{iFt}c_i^\dagger c_{i+1} + h.c.\right) + Q_1(-1)^i c_i^\dagger c_i + Q_1'(-1)^i\left(e^{2iFt}c_i^\dagger c_{i+2} + h.c.\right) \quad (30)$$

where Q_1 is the staggered onsite energy and Q_2 is the bond strength alternation. Note that the inversion symmetry is broken in the presence of both Q_1 and Q_2. This model describes the 1D organic conductors (*33*–*36*). This is also the simplest model of ferroelectricity in perovskite materials, where Q_1 corresponds to the energy level difference between the oxygen and metal ions and Q_2 corresponds to the bond strength change due to the displacement of the ions (*37*). To see the effect of T-symmetry breaking, we also introduced Q_1', which expresses complex hoppings between next-nearest neighbors having opposite signs for two sublattices. The Hamiltonian in Eq. 30 is given in the k-space as

$$H_0 = \cos\frac{k}{2}\sigma_x + Q_2 \sin\frac{k}{2}\sigma_y + \left(Q_1 + Q_1'\sin k\right)\sigma_z \quad (31)$$

where $\boldsymbol{\sigma} = (\sigma_x, \sigma_y, \sigma_z)$ are the Pauli matrices describing the degree of freedom of the two sublattices in the unit cell. Now, let us apply an electric field E to this 1D model. The Floquet Hamiltonian is given by

$$H_{mn}(k) = \begin{pmatrix} Q_1 - n\Omega & 0 \\ 0 & -Q_1 - n\Omega \end{pmatrix}\delta_{mn} + \begin{pmatrix} C_{mn} & A_{mn} \\ B_{mn} & -C_{mn} \end{pmatrix} \quad (32)$$

with $A_{mn} = (t + Q_2/2)e^{-ik/2}J_{m-n}(-F/2) + (t - Q_2/2)e^{ik/2}J_{m-n}(F/2)$, $B_{mn} = (t + Q_2/2)e^{ik/2}J_{m-n}(F/2) + (t - Q_2/2)e^{-ik/2}J_{m-n}(-F/2)$, and $C_{mn} = Q_1'J_{m-n}(F)(-i)^{m-n}[(-1)^{m-n}e^{ik} - e^{-ik}]/(2i)$, where $F = eEa/\Omega$ with lattice spacing a, and $J_n(x)$ is the nth Bessel function.

We can define R_{Q_2} similar to R_k in Eq. 14 by replacing the k-derivative with a Q_2-derivative. Then, we can consider the 2D vector field $\tilde{\boldsymbol{\mathcal{A}}}(k, Q_2) = (\tilde{\mathcal{A}}_k, \tilde{\mathcal{A}}_{Q_2}) = |v_{12}^0|^2(R_k, R_{Q_2})$ in the (k,Q_2)-plane as plotted in Fig. 2. Taking the rotation of the vector field $\boldsymbol{R}$, one can get the flux distribution $\tilde{\mathcal{F}} = |v_{12}^0|^2(\partial_k R_{Q_2} - \partial_{Q_2}R_k) = |v_{12}^0|^2\mathcal{F}$ in the inset of Fig. 2. We note that $\tilde{\mathcal{F}}$ is $|v_{12}^0|^2$ times the difference $\mathcal{F} \equiv \mathcal{F}_2 - \mathcal{F}_1$ between the Berry curvatures of conduction and valence bands since the contribution from the phase of the transition matrix elements drops. These plots provide various information as follows. First, the sum of A_k at k and $-k$ satisfying the energy conservation law $E_2(\boldsymbol{k}) - E_1(\boldsymbol{k}) = \hbar\omega$ (indicated by two red dots in Fig. 2) corresponds to the shift current J proportional to E^2. Note that this sum does not vanish when Q_2 is nonzero, that is, P-symmetry is broken. The corresponding quantity for $\tilde{\mathcal{A}}_{Q_2}$ gives the change in the bond dimerization $B = \Sigma_i(-1)^i(c_i^\dagger c_{i+1} + h.c.)$, which is the "current" corresponding to the "vector potential" Q_2. However, as seen from Fig. 2, the contributions from k and $-k$ always cancel due to the T-symmetry.

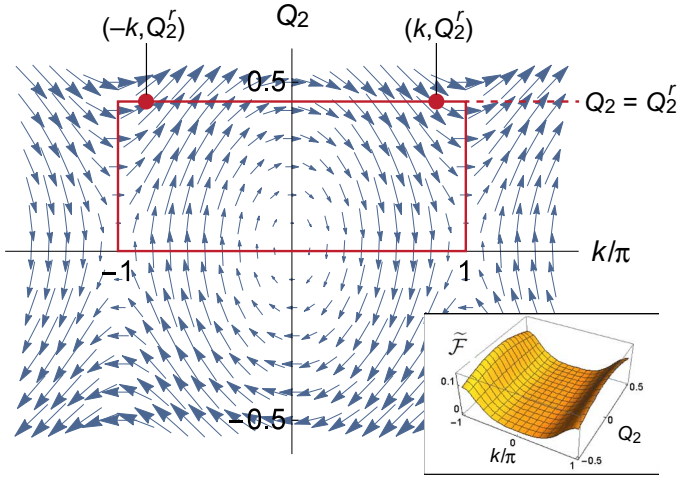

Fig. 2. Vector field $\tilde{\mathcal{A}}$ for the 1D model, which preserves TRS and breaks inversion symmetry. We plot $(\tilde{\mathcal{A}}_k, \tilde{\mathcal{A}}_{Q_2})$ in the parameter space (k, Q_2) with $Q_1 = 1$, $Q_1' = 0$. Inset is a plot of distribution of the "flux" $\tilde{\mathcal{F}}$ defined in the text, which is related to the third-order nonlinear responses.

Let us now turn to the Berry curvature. The integral of $\mathcal{F}$ over the "first Brillouin zone" $-\pi < k < \pi, 0 < Q_2 < Q_2^r$ (Q_2^r is the realized value of the bond alternation), which is denoted by a red square in Fig. 2, is related to the polarization (*12*). Namely, the integral of $\mathcal{F}_1$ over the first Brillouin zone is the polarization of the ground state. Therefore, that of $\mathcal{F}$ is the change of the polarization when all the electrons in the valence band are excited to the conduction band. The value of $\tilde{\mathcal{F}}$ is related to the change in the bond dimerization B defined above, which is proportional to E^3. This third-order nonlinear response of B will be obtained if k_y is replaced by Q_2 in Eqs. 28 and 29 and if the integration over Q_2 is dropped. This is intuitively understood as a "Hall response" of B, which is the current with respect to Q_2 and is transverse to the k-direction. In this case, there is no Q_2 integration because the contribution arises only from the realized value Q_2^r, and the photo-induced change of B is given by the sum of $\mathcal{F}$ at (k, Q_2^r) and $(-k, Q_2^r)$ with $\pm k$, satisfying the energy conservation law (indicated by two red dots in Fig. 2). As shown in the inset of Fig. 2, the values of $\mathcal{F}$ at k and $-k$ are equal to each other, and hence, this sum becomes nonvanishing. It is useful to note here that there is a very sensitive probe of B in the case of molecular solids. The frequency shift of the intramolecular vibrations detects the change of the valence state of each molecule (*38*). We note that an antivortex in vector field $\tilde{\boldsymbol{\mathcal{A}}}$ at $(k, Q_2) = (\pm\pi, 0)$ is attributed to the peak of the Berry curvature, whereas a vortex at $(k, Q_2) = (0, 0)$ arises from the singularity in v_{12}^0, where v_{12}^0 vanishes and its phase is not well defined.

Next, we consider the effects of broken TRS T. Figure 3A shows plots similar to those in Fig. 2 with finite $Q_1' = 0.1$. It is clear that the symmetry between k and $-k$ is broken, and hence, all the effects discussed above can be nonvanishing. For example, the photo-induced

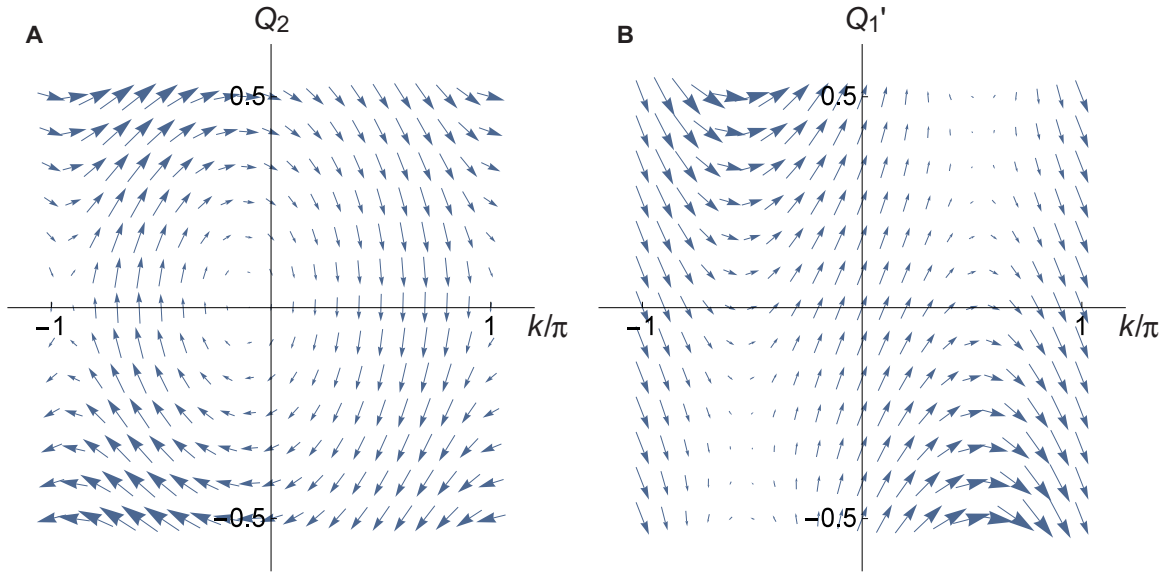

Fig. 3. Vector fields $\tilde{\mathcal{A}}$ for the 1D model, which break both TRS and inversion symmetry. (**A** and **B**) We plot $(\tilde{\mathcal{A}}_k, \tilde{\mathcal{A}}_{Q_2})$ with $Q_1 = 1$, $Q_1' = 0.1$ (A) and $(\tilde{\mathcal{A}}_k, \tilde{\mathcal{A}}_{Q_1'})$ with $Q_1 = 1$, $Q_2 = 0.4$ (B).

change in the bond dimerization proportional to E^2 becomes nonzero in addition to the shift current. We note that there is symmetry between Q_2 and $-Q_2$, which originates from the PT-symmetry, as discussed in the next section. Figure 3B shows the vector field $(\tilde{\mathcal{A}}_k, \tilde{\mathcal{A}}_{Q_1'})$ with fixed $Q_1 = 1$, $Q_2 = 0.4$. Although nonzero Q_1 and Q_2 break the P-symmetry, this figure demonstrates the role of T-symmetry. Namely, both Q_1' and k change their sign under T, and the vector field in Fig. 3B obeys the constraint of the T-symmetry. The symmetry properties of various quantities will be discussed in the next section.

DISCUSSION

Symmetry considerations

On the basis of the results presented in the previous section, it is useful to summarize the symmetry properties. Figure 4 shows the transformation laws of the various quantities with respect to P and T. Here, the parameter Q breaks P-symmetry and reverses its sign under the P operation, whereas it remains unchanged under T. This is the case for Q_2 in the model Eq. 30. On the other hand, $\boldsymbol{k}$ goes to $-\boldsymbol{k}$ for both P and T. The parameter Q_1' is also odd under both P and T. The transformation properties of the Berry connection and the Berry curvature are summarized in Fig. 4. In particular, the presence or absence of the T-symmetry determines whether the effect of interest is allowed.

Let us study these transformation properties of $\tilde{\mathcal{A}}$ and $\tilde{\mathcal{F}}$ in the 1D model in Eq. 30 below. First, we discuss symmetry constraints on the vector fields in the T-symmetric case shown in Fig. 2. The action of T constrains the vector field as $(\tilde{\mathcal{A}}_k(-k, Q_2), \tilde{\mathcal{A}}_{Q_2}(-k, Q_2)) = (\tilde{\mathcal{A}}_k(k, Q_2), -\tilde{\mathcal{A}}_{Q_2}(k, Q_2))$, which is satisfied by two vectors at the two red dots in Fig. 2. Because the nonlinear responses are both contributed from (k, Q_2) and $(-k, Q_2)$, the presence of the T-symmetry allows nonzero response associated with $\tilde{\mathcal{A}}_k$ (shift current) but excludes that with $\tilde{\mathcal{A}}_{Q_2}$ (nonlinear bond dimerization). Similarly, the vector field in Fig. 2 is consistent with the constraint of the P-symmetry given by $(\tilde{\mathcal{A}}_k(-k, -Q_2), \tilde{\mathcal{A}}_{Q_2}(-k, -Q_2)) = (-\tilde{\mathcal{A}}_k(k, Q_2), -\tilde{\mathcal{A}}_{Q_2}(k, Q_2))$. Because the flux distribution $\tilde{\mathcal{F}}_{kQ_2}$ in the parameter space (k, Q_2) is even under both T and P, as seen in the inset, and because the contributions at k and $-k$ always add up, nonvanishing third-order nonlinear response associated with $\tilde{\mathcal{F}}_{kQ}$ is allowed. (We note that the nonlinear Kerr response is not allowed by the T-symmetry because contributions to $\tilde{\mathcal{F}}_{k_xk_y}$ from k and $-k$ cancel out.) Next, we consider the cases in Fig. 3 where the T-symmetry is broken due to the nonzero Q_1'. The vector field in Fig. 3A is not closed under the action of either T or P because the fixed parameter Q_1' changes its sign, but it is closed under the combined PT-symmetry. From Fig. 4, the vector fields are constrained by the PT-symmetry as $(\tilde{\mathcal{A}}_k(-k, -Q_1'), \tilde{\mathcal{A}}_{Q_1'}(-k, -Q_1')) = (\tilde{\mathcal{A}}_k(k, Q_1'), \tilde{\mathcal{A}}_{Q_1'}(k, Q_1'))$, which is consistent with Fig. 3A. In this case, both nonlinear responses associated with $\tilde{\mathcal{A}}_k$ and $\tilde{\mathcal{A}}_{Q_2}$ are allowed because the T-symmetry is no longer present. The vector field in Fig. 3B is not closed under the action of P because the fixed parameter Q_2 changes its sign under P but is closed under the action of T; the T-symmetry constrains the vector field in Fig. 3B. Under the action of T, the Berry connections $\tilde{\mathcal{A}}_k$ and $\tilde{\mathcal{A}}_{Q_1'}$ are even as seen from Fig. 4. Thus, the vector fields transform as $(\tilde{\mathcal{A}}_k(-k, -Q_1'), \tilde{\mathcal{A}}_{Q_1'}(-k, -Q_1')) = (\tilde{\mathcal{A}}_k(k, Q_1'), \tilde{\mathcal{A}}_{Q_1'}(k, Q_1'))$, which is consistent with Fig. 3B.

CONCLUSIONS

We studied NLORs from the topological properties based on the Keldysh Green's function method combined with the Floquet formalism, taking into account the two states connected by the optical transition. The Berry connection and the Berry curvature appear in the even- and odd-order responses in the electric field E of the light, respectively. For example, the shift current proportional to E^2 is represented by the Berry connection, whereas the Berry curvature appears in the third-order response in E. These processes involve the excitation of electrons from the valence band to the conduction band, where created electrons

	T	P	PT
$\widetilde{\mathcal{A}}_k$	+	−	−
$\widetilde{\mathcal{A}}_Q$	−	−	+
$\widetilde{\mathcal{F}}_{k_x k_y}$	−	+	−
$\widetilde{\mathcal{F}}_{kQ}$	+	+	+

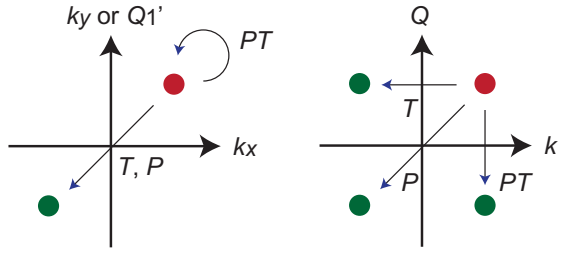

Fig. 4. Transformation laws of Berry connection and Berry curvature. We consider the geometry in the space spanned by the momentum k and the parameter Q quantifying the inversion breaking and the geometry in the momentum space with k_x and k_y (or Q_1'). Here, Q is even under T, whereas k and Q_1' are odd under T. All Q, Q_1' and k are odd under P.

and holes have been assumed to be noninteracting in this paper. In real materials, however, the electron correlation effect should be taken into account. In particular, the excitonic effect will hinder photocurrent generation. Therefore the many-body formulation of NLORs is an important issue to be studied in the future. As for ferroelectric materials, however, the large dielectric constant screens the Coulomb effect, and the excitonic effect is suppressed, which may justify single-particle treatment.

MATERIALS AND METHODS

Keldysh Green's function

The Keldysh Green's function in the Floquet formalism is given by the Dyson equation (*23*, *28*, *29*, *31*)

$$\begin{pmatrix} G^{\mathrm{R}} & G^{\mathrm{K}} \\ 0 & G^{\mathrm{A}} \end{pmatrix}^{-1}_{mn} = \begin{pmatrix} (\omega + n\Omega)\delta_{mn} - H_{mn} & 0 \\ 0 & (\omega + n\Omega)\delta_{mn} - H_{mn} \end{pmatrix} + \Sigma_{mn} \quad (33)$$

where m, n run over the Floquet indices, and Σ is the self-energy. The Floquet Hamiltonian H was obtained by expanding a Hamiltonian $H(t)$ periodic in time with period T in the Floquet modes as

$$H_{mn} = \frac{1}{T}\int_0^T dt e^{i(m-n)\Omega t} H_0(t) \quad (34)$$

with $\Omega = 2\pi/T$. We assumed that each site was coupled to a heat reservoir with the Fermi distribution function $f(\epsilon)$ with a coupling constant Γ. In this case, the self-energy is written as

$$\Sigma_{mn} = i\Gamma\delta_{mn}\begin{pmatrix} \frac{1}{2} & -1 + 2f(\omega + m\Omega) \\ 0 & -\frac{1}{2} \end{pmatrix} \quad (35)$$

Then, the current is given by

$$J(t) = \sum_m -i\mathrm{Tr}[v(t)G^<_{mn}]e^{-i(m-n)\Omega t} \quad (36)$$

where $v(t)$ is the time-dependent velocity operator defined by $v(t) = \partial H_0(t)/\partial k$ and Tr denotes an integration over k and ω and a trace over band indices (but not over Floquet indices). We noted that the reference Floquet index n could be arbitrarily chosen because of the translation symmetry in the Floquet index. The lesser Green's function $G^<$ is given by

$$G^< = G^{\mathrm{R}}\Sigma^< G^{\mathrm{A}} \quad (37)$$

$$\Sigma^< = \frac{\Sigma^{\mathrm{R}} + \Sigma^{\mathrm{K}} - \Sigma^{\mathrm{A}}}{2} \quad (38)$$

We noted that the retarded and advanced Green's functions are simply written as

$$(G^{\mathrm{R/A}})^{-1}_{mn} = \left(\omega + n\Omega \pm \frac{i\Gamma}{2}\right)\delta_{mn} - H_{mn} \quad (39)$$

Furthermore, the dc part of the current J is concisely obtained from the dc current operator defined from the Floquet Hamiltonian as

$$J = \sum_m -i\mathrm{Tr}[\tilde{v}_{nm}G^<_{mn}] \quad (40)$$

$$\tilde{v} = \frac{\partial H_F}{\partial k} \quad (41)$$

Lesser Green's function for the Floquet two-band model

In this section, we focused on the Floquet two-band model and studied the lesser Green's function that is directly related to physical quantities.

First, we derived the Floquet Hamiltonian H_{F} starting from the original Hamiltonian without a drive $H_{\mathrm{orig}}(k)$. In the presence of the monochromatic light $E(t) = Ee^{-i\Omega t} + E^* e^{i\Omega t}$, the time-dependent Hamiltonian is given by

$$H_0(t) = H_{\mathrm{orig}}\Big(k + A(t)\Big) \quad (42)$$

$$A(t) = iAe^{-i\Omega t} - iA^* e^{i\Omega t} \quad (43)$$

with $A = E/\Omega$. By keeping terms up to the linear order in A, one obtains

$$H_0(t) \cong H_{\mathrm{orig}}(k) + A(t)v^0 \tag{44}$$

with $v^0 = \partial H_{\mathrm{orig}}/\partial k$. Next, we expressed this time-dependent Hamiltonian as a Floquet Hamiltonian $(H_F)_{mn} = H_{mn} - n\Omega\delta_{mn}$ by using Eq. 34. We further focused on two Floquet bands, that is, the valence band with the Floquet index $n = -1$ and the conduction band with the Floquet index $n = 0$. This led to the two-by-two Floquet Hamiltonian

$$H_F = \begin{pmatrix} \epsilon_1^0 + \Omega & -iA^* v_{12}^0 \\ iAv_{21}^0 & \epsilon_2^0 \end{pmatrix} \equiv \epsilon + \boldsymbol{d}\cdot\boldsymbol{\sigma} \tag{45}$$

where subscripts 1 and 2 refer to the valence band and conduction band, respectively, and $\epsilon_i^0 = (H_{\mathrm{orig}})_{ii}$.

For this two-by-two Floquet Hamiltonian, the lesser Green's function $G^<$ was obtained as follows. We considered the case where a coupling to a heat bath leads to the self-energy given by Eq. 35. In this case, the retarded and advanced Green's functions are written as

$$G^{\mathrm{R/A}} = \frac{\omega - \epsilon \pm i\Gamma/2 + \boldsymbol{d}\cdot\boldsymbol{\sigma}}{(\omega - \epsilon \pm i\Gamma/2)^2 - d^2} \tag{46}$$

Because the Fermi energy of the bath lies within the energy gap of the system, the Keldysh component of the self-energy reduces to

$$\Sigma^< = i\Gamma\frac{1+\sigma_z}{2} \tag{47}$$

With these data, the lesser Green's function for the Floquet two band model was obtained from Eq. 38. For example, an off-diagonal element of $G^<$ is given by

$$(G^<)_{21} = \frac{(d_x + id_y)\left(\frac{\Gamma}{2} + id_z\right)}{2\left(d^2 + \frac{\Gamma^2}{4}\right)} \tag{48}$$

Here, we noted that the superscript 21 indicates bases of the two-by-two Hamiltonian H_F (with corresponding Floquet indices 0, −1), and $(G^<)_{21}$ describes the Fourier component of $e^{-i\Omega t}$ according to Eq. 36.

Moreover, general expectation values are written as

$$\begin{aligned}\langle b_0 + \boldsymbol{b}\cdot\boldsymbol{\sigma}\rangle &= -i\mathrm{Tr}[(b_0 + \boldsymbol{b}\cdot\boldsymbol{\sigma})G^<] \\ &= \frac{1}{d^2 + \frac{\Gamma^2}{4}}\left[\frac{\Gamma}{2}\left(-d_x b_y + d_y b_x\right) + \left(d_x b_x + d_y b_y\right)d_z \right. \\ &\qquad \left. + \left(d_z^2 + \frac{\Gamma^2}{4}\right)b_z\right] + b_0 \end{aligned} \tag{49}$$

REFERENCES AND NOTES

1. N. Bloembergen, *Nonlinear Optics* (World Scientific, Singapore, ed. 4, 1996).
2. R. W. Boyd, *Nonlinear Optics* (Academic Press, London, ed. 3, 2008).
3. I. Grinberg, D. V. West, M. Torres, G. Gou, D. M. Stein, L. Wu, G. Chen, E. M. Gallo, A. R. Akbashev, P. K. Davies, J. E. Spanier, A. M. Rappe, Perovskite oxides for visible-light-absorbing ferroelectric and photovoltaic materials. *Nature* **503**, 509–512 (2013).
4. W. Nie, H. Tsai, R. Asadpour, J.-C. Blancon, A. J. Neukirch, G. Gupta, J. J. Crochet, M. Chhowalla, S. Tretiak, M. A. Alam, H.-L. Wang, A. D. Mohite, High-efficiency solution-processed perovskite solar cells with millimeter-scale grains. *Science* **347**, 522–525 (2015).
5. D. Shi, V. Adinolfi, R. Comin, M. Yuan, E. Alarousu, A. Buin, Y. Chen, S. Hoogland, A. Rothenberger, K. Katsiev, Y. Losovyj, X. Zhang, P. A. Dowben, O. F. Mohammed, E. H. Sargent, O. M. Bakr, Low trap-state density and long carrier diffusion in organolead trihalide perovskite single crystals. *Science* **347**, 519–522 (2015)
6. D. W. de Quilettes, S. M. Vorpahl, S. D. Stranks, H. Nagaoka, G. E. Eperon, M. E. Ziffer, H. J. Snaith, D. S. Ginger, Impact of microstructure on local carrier lifetime in perovskite solar cells. *Science* **348**, 683–686 (2015).
7. A. Bhatnagar, A. R. Chaudhuri, Y. H. Kim, D. Hesse, M. Alexe, Role of domain walls in the abnormal photovoltaic effect in $BiFeO_3$. *Nat. Commun.* **4**, 2835 (2013).
8. R. von Baltz, W. Kraut, Theory of the bulk photovoltaic effect in pure crystals. *Phys. Rev. B* **23**, 5590–5596 (1981).
9. S. M. Young, A. M. Rappe, First principles calculation of the shift current photovoltaic effect in ferroelectrics. *Phys. Rev. Lett.* **109**, 116601 (2012).
10. S. M. Young, F. Zheng, A. M. Rappe, First-principles calculation of the bulk photovoltaic effect in bismuth ferrite. *Phys. Rev. Lett.* **109**, 236601 (2012).
11. A. M. Cook, B. M. Fregoso, F. de Juan, J. E. Moore, Design principles for shift current photovoltaics. arXiv:1507.08677 (2015).
12. R. Resta, Macroscopic polarization in crystalline dielectrics: The geometric phase approach. *Rev. Mod. Phys.* **66**, 899–915 (1994).
13. D. J. Thouless, M. Kohmoto, M. P. Nightingale, M. den Nijs, Quantized hall conductance in a two-dimensional periodic potential. *Phys. Rev. Lett.* **49**, 405–408 (1982).
14. D. J. Thouless, Quantization of particle transport. *Phys. Rev. B* **27**, 6083–6087 (1983).
15. N. Nagaosa, J. Sinova, S. Onoda, A. H. MacDonald, N. P. Ong, Anomalous hall effect. *Rev. Mod. Phys.* **82**, 1539–1592 (2010).
16. S. Murakami, N. Nagaosa, S.-C. Zhang, Dissipationless quantum spin current at room temperature. *Science* **301**, 1348–1351 (2003).
17. J. Sinova, D. Culcer, Q. Niu, N. A. Sinitsyn, T. Jungwirth, A. H. MacDonald, Universal intrinsic spin hall effect. *Phys. Rev. Lett.* **92**, 126603 (2004).
18. M. Z. Hasan, C. L. Kane, Colloquium: Topological insulators. *Rev. Mod. Phys.* **82**, 3045–3067 (2010).
19. X.-L. Qi, S.-C. Zhang, Topological insulators and superconductors. *Rev. Mod. Phys.* **83**, 1057 (2011).
20. C.-K. Chiu, J. C. Y. Teo, A. P. Schnyder, S. Ryu, Classification of topological quantum matter with symmetries. arXiv:1505.03535 (2015).
21. B. Hetényi, dc conductivity as a geometric phase. *Phys. Rev. B* **87**, 235123 (2013).
22. E. N. Adams, E. I. Blount, Energy bands in the presence of an external force field—II: Anomalous velocities. *J. Phys. Chem. Sol.* **10**, 286–303 (1959).
23. T. Oka, H. Aoki, Photovoltaic Hall effect in graphene. *Phys. Rev. B* **79**, 081406(R) (2009).
24. T. Kitagawa, T. Oka, A. Brataas, L. Fu, E. Demler, Transport properties of nonequilibrium systems under the application of light: Photoinduced quantum Hall insulators without Landau levels. *Phys. Rev. B* **84**, 235108 (2011).
25. M. A. Sentef, M. Claassen, A. F. Kemper, B. Moritz, T. Oka, J. K. Freericks, T. P. Devereaux, Theory of Floquet band formation and local pseudospin textures in pump-probe photoemission of graphene. *Nat. Commun.* **6**, 7047 (2015).
26. J. W. McIver, D. Hsieh, H. Steinberg, P. Jarillo-Herrero, N. Gedik, Control over topological insulator photocurrents with light polarization. *Nat. Nanotechnol.* **7**, 96–100 (2012).
27. G. Jotzu, M. Messer, R. Desbuquois, M. Lebrat, T. Uehlinger, D. Greif, T. Esslinger, Experimental realization of the topological Haldane model with ultracold fermions. *Nature* **515**, 237–240 (2014).
28. S. Kohler, J. Lehmann, P. Hänggi, Driven quantum transport on the nanoscale. *Phys. Rep.* **406**, 379–443 (2005).
29. A.-P. Jauho, N. S. Wingreen, Y. Meir, Time-dependent transport in interacting and noninteracting resonant-tunneling systems. *Phys. Rev. B* **50**, 5528–5544 (1994).
30. K. Johnsen, A.-P. Jauho, Quasienergy spectroscopy of excitons. *Phys. Rev. Lett.* **83**, 1207–1210 (1999).
31. A. Kamenev, Many-body theory of non-equilibrium systems. arXiv:0412296 (2004).
32. J. E. Sipe, A. I. Shkrebtii, Second-order optical response in semiconductors. *Phys. Rev. B* **61**, 5337–5352 (2000).
33. W. P. Su, J. R. Schrieffer, A. J. Heeger, Soliton excitations in polyacetylene. *Phys. Rev. B* **22**, 2099–2111 (1980).
34. M. J. Rice, E. J. Mele, Elementary excitations of a linearly conjugated diatomic polymer. *Phys. Rev. Lett.* **49**, 1455–1459 (1982).
35. N. Nagaosa, J.-. Takimoto, Theory of neutral-ionic transition in organic crystals. I. Monte Carlo simulation of modified Hubbard model. *J. Phys. Soc. Jpn.* **55**, 2735–2744 (1986).
36. S. Onoda, S. Murakami, N. Nagaosa, Topological nature of polarization and charge pumping in ferroelectrics. *Phys. Rev. Lett.* **93**, 167602 (2004).
37. T. Egami, S. Ishihara, M. Tachiki, Lattice effect of strong electron correlation: Implication for ferroelectricity and superconductivity. *Science* **261**, 1307–1310 (1993).

38. Y. Tokura, T. Koda, G. Saito, T. Mitani, Effect of substitutional impurities on the neutral-to-ionic phase transition in TTF-*p*-chloranil crystal. *J. Phys. Soc. Jpn.* **53**, 4445–4455 (1984).

Acknowledgments: We thank Y. Tokura, M. Kawasaki, N. Ogawa, J. E. Moore, J. Orenstein, and B. M. Fregoso for fruitful discussions. **Funding:** This work was supported by the Emergent Phenomena in Quantum Systems initiative of the Gordon and Betty Moore Foundation (T.M.), by the Japan Society for the Promotion of Science Grant-in-Aid for Scientific Research (nos. 24224009 and 26103006) from the Ministry of Education, Culture, Sports, Science and Technology, Japan, and by the ImPACT (Impulsing Paradigm Change through Disruptive Technologies) Program of Council for Science, Technology and Innovation (Cabinet office, Government of Japan) (N.N.). **Author contributions:** T.M. and N.N. performed the calculations and wrote the manuscript. **Competing interests:** The authors declare that they have no competing interests. **Data and materials availability:** All data needed to evaluate the conclusions in the paper are present in the paper and/or the Supplementary Materials. Additional data related to this paper may be requested from the authors.

Submitted 27 October 2015
Accepted 20 April 2016
Published 20 May 2016
10.1126/sciadv.1501524

Citation: T. Morimoto, N. Nagaosa, Topological nature of nonlinear optical effects in solids. *Sci. Adv.* **2**, e1501524 (2016).

Topological nature of nonlinear optical effects in solids

Takahiro Morimoto and Naoto Nagaosa

Sci Adv **2** (5), e1501524.
DOI: 10.1126/sciadv.1501524